Frontiers of Information Technology & Electronic Engineering
www.jzus.zju.edu.cn; engineering.cae.cn; www.springerlink.com
ISSN 2095-9184 (print); ISSN 2095-9230 (online)
E-mail: jzus@zju.edu.cn

Target height and multipath attenuation joint estimation with complex scenarios for very high frequency radar*

Sheng CHEN, Yongbo ZHAO†‡, Yili HU, Chenghu CAO, Xiaojiao PANG

National Laboratory of Radar Signal Processing, Xidian University, Xi'an 710071, China

†E-mail: ybzhao@xidian.edu.cn

Received Jan. 4, 2021; Revision accepted Mar. 31, 2021; Crosschecked Jan. 12, 2022; Published online Apr. 29, 2022

Abstract: Low-angle estimation for very high frequency (VHF) radar is a difficult problem due to the multipath effect in the radar field, especially in complex scenarios where the reflection condition is unknown. To deal with this problem, we propose an algorithm of target height and multipath attenuation joint estimation. The amplitude of the surface reflection coefficient is estimated by the characteristic of the data itself, and it is assumed that there is no reflected signal when the amplitude is very small. The phase of the surface reflection coefficient and the phase difference between the direct and reflected signals are searched as the same part, and this represents the multipath phase attenuation. The Cramer-Rao bound of the proposed algorithm is also derived. Finally, computer simulations and real data processing results show that the proposed algorithm has good estimation performance under complex scenarios and works well with only one snapshot.

Key words: Low-angle estimation; Very high frequency (VHF) radar; Complex scenarios; Multipath effect; Height estimation
https://doi.org/10.1631/FITEE.2100003 **CLC number:** TN95

1 Introduction

In recent decades, the problem of low-angle estimation for very high frequency (VHF) radar has attracted a lot of attention (Barton, 1974; Bosse et al., 1991; Xu et al., 2013, 2014) because of the multipath effect, especially in complex scenarios (Wang et al., 2014) where the reflection condition is unknown. The direct and reflected signals passing along the Earth's surface enter the radar main beam together. It is assumed that only the specular reflection signal is included in the reflected path signals, while the diffuse reflection signal can be ignored (Bosse et al., 1991). The target height is calculated from the elevation angle and other information about the target, which is known for the height estimation, so the height estimation is equivalent to the elevation estimation. The direct and reflected signals cannot be distinguished in the time, Doppler, and space domains, resulting in degradation of target height estimation performance. In particular, the performance for complex scenarios is greatly reduced.

Subspace and maximum likelihood (ML) algorithms are currently the main methods to overcome this problem. Subspace algorithms such as music (Schmidt, 1986) and esprit (Roy and Kailath, 1989) usually require more snapshots, and cannot directly deal with coherent signals. Spatial smoothing (Shan et al., 1985; Pillai and Kwon, 1989) can help reduce the coherence between the signals by losing a certain aperture before angle estimation. ML algorithms (Ziskind and Wax, 1988) can directly process coherent signals and can work even with only one snapshot. The refined maximum likelihood (RML) algorithm

‡ Corresponding author
* Project supported by the Fund for Foreign Scholars in University Research and Teaching Programs (the 111 Project) (No. B18039)
ORCID: Sheng CHEN, https://orcid.org/0000-0003-3519-1137; Yongbo ZHAO, https://orcid.org/0000-0002-6453-0786

(Lo and Litva, 1991) makes full use of the prior knowledge of geometric information and the surface reflection coefficient, and uses a composite guide vector instead of a conventional guide vector. The RML algorithm performs well in simple scenarios where the reflection condition is known precisely, but not well in complex scenarios. The reflected signal can also be eliminated (Ahn et al., 2010; Park et al., 2014), but the information about the space domain in the reflected signal is lost. In Takahashi et al. (2010) and Wang et al. (2016), the height of the reflector is treated as an unknown parameter, and is searched together with the target height. Thus, the sensitivity to the fluctuation of the reflector is reduced. However, the error of the surface reflection coefficient is not taken into account. In complex scenarios, the composite guide vector cannot be accurately calculated, resulting in performance degradation and even failure of the above algorithms. To overcome these problems, we propose an algorithm of target height and multipath attenuation joint estimation. This study considers the case of low antenna height and a far field target. The reflected signal is thought of as symmetric with respect to the horizontal plane of the direct signal. The amplitude of the surface reflection coefficient is estimated by the characteristic of the data itself, and it is considered that there is no reflected signal when the amplitude is very small. The phase of the surface reflection coefficient and the phase difference between the direct and reflected signals are searched as the same part, and this is the multipath phase attenuation. An alternating projection (AP) is used to reduce computation by iterative processing (Ziskind and Wax, 1988; Heylen et al., 2016). The proposed algorithm fully exploits the characteristics of data in complex scenarios and improves the performance of target height estimation.

2 Multipath signal model based on 4/3 Earth

In this section, we give the multipath signal model based on 4/3 Earth and briefly review the surface reflection coefficient.

2.1 Multipath signal model

Electromagnetic waves do not travel along a straight line on the Earth. This is because of the effects of the Earth's atmosphere and its curved surface (Ayasli, 1986; Teti, 2000; Griesser and Balanis, 2003). However, it can be equivalent to traveling along a straight line with appropriate approximation. Using the 4/3 Earth model (Beckmann and Spizzichino, 1987; Mahafza, 2013), the effective Earth radius is

$$R_e = 4R_0/3, \tag{1}$$

where R_0 is real Earth radius. Based on the above approximation, the geometry for a 4/3 Earth model with multipath propagation is shown in Fig. 1. The linear array with the M elements receives the two paths of signal echoes from the different directions of arrival. One path returns directly from the target to the radar antenna, whereas the other path returns from the reflecting surface, where θ_1 and θ_2 are the incident angles of the direct signal and the reflected signal, respectively. The height of the array radar center is h_r. The distance between two adjacent array elements is d. The height of the target is h_t. The distance from the target to the array radar center is R_d.

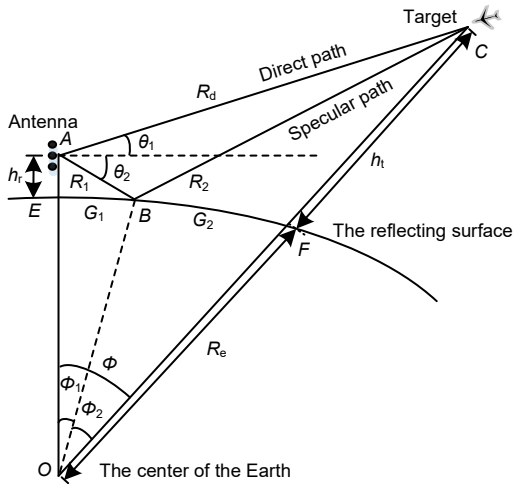

Fig. 1 Geometry for a 4/3 Earth model with multipath propagation

After pulse compression and Doppler filtering, the signal received by array radar can be written as

$$\boldsymbol{x} = \alpha \boldsymbol{w} + \boldsymbol{n}, \tag{2}$$

$$\boldsymbol{w} = \boldsymbol{a}(\theta_1) + \varepsilon \boldsymbol{a}(\theta_2), \tag{3}$$

where α is the complex amplitude related to target characteristics, $\boldsymbol{w}$ is the composite array steering

vector including direct and reflected signals, and $\boldsymbol{a}(\theta)\in\mathbb{C}^M$, called the array steering vector, is defined as

$$\boldsymbol{a}(\theta)=\left[\mathrm{e}^{\frac{-\mathrm{j}\pi d(M-1)\sin\theta}{\lambda}},\mathrm{e}^{\frac{-\mathrm{j}\pi d(M-3)\sin\theta}{\lambda}},\cdots,\mathrm{e}^{\frac{\mathrm{j}\pi d(M-1)\sin\theta}{\lambda}}\right]^{\mathrm{T}}, \quad (4)$$

where λ is the working wavelength, and ε is the attenuation coefficient, satisfying

$$\varepsilon=\rho\mathrm{e}^{-\mathrm{j}\varphi}=\rho\exp\left(-\frac{\mathrm{j}2\pi\Delta R}{\lambda}\right), \quad (5)$$

where ρ is the surface reflection coefficient. The details of ρ will be discussed later. φ is the phase difference between the direct and reflected signals, and ΔR is the wave path difference between the direct and reflected signals. $\boldsymbol{n}$ is the Gaussian white noise vector with zero mean. This is not correlated with the target signals. The variance matrix of the noise vector is $\sigma^2\boldsymbol{I}_M$. σ^2 represents the noise power of a single array element, and $\boldsymbol{I}_M$ represents an identity matrix of size $M\times M$. In addition, from the multipath geometry in Fig. 1, we give the calculation of θ_2 and ΔR. The height of the target is

$$h_{\mathrm{t}}=\sqrt{R_{\mathrm{d}}^2+(R_{\mathrm{e}}+h_{\mathrm{r}})^2-2R_{\mathrm{d}}(R_{\mathrm{e}}+h_{\mathrm{r}})\cos\left(\theta_1+\frac{\pi}{2}\right)}-R_{\mathrm{e}}. \quad (6)$$

The angle Φ is

$$\Phi=\Phi_1+\Phi_2=\arccos\frac{(R_{\mathrm{e}}+h_{\mathrm{r}})^2+(R_{\mathrm{e}}+h_{\mathrm{t}})^2-R_{\mathrm{d}}^2}{2(R_{\mathrm{e}}+h_{\mathrm{r}})(R_{\mathrm{e}}+h_{\mathrm{t}})}. \quad (7)$$

The length of the arc $\overset{\frown}{EF}$ is

$$G=R_{\mathrm{e}}\Phi. \quad (8)$$

The length of the arc $\overset{\frown}{EB}$ (Skolnik, 2008) is

$$G_1=\frac{G}{2}-p\sin\frac{\xi}{3}, \quad (9)$$

where

$$p=\frac{2}{\sqrt{3}}\sqrt{R_{\mathrm{e}}(h_{\mathrm{r}}+h_{\mathrm{t}})+\frac{G^2}{4}}, \quad (10)$$

$$\xi=\arcsin\frac{2R_{\mathrm{e}}G(h_{\mathrm{t}}-h_{\mathrm{r}})}{p^3}. \quad (11)$$

The angles Φ_1 and Φ_2 are

$$\Phi_1=\frac{G_1}{R_{\mathrm{e}}}, \quad (12)$$

$$\Phi_2=\frac{G_2}{R_{\mathrm{e}}}=\frac{G-G_1}{R_{\mathrm{e}}}. \quad (13)$$

Then, R_1 and R_2 can be calculated by $\triangle OAB$ and $\triangle OBC$. We have

$$R_1=\sqrt{R_{\mathrm{e}}^2+\left(R_{\mathrm{e}}+h_{\mathrm{r}}\right)^2-2R_{\mathrm{e}}\left(R_{\mathrm{e}}+h_{\mathrm{r}}\right)\cos\Phi_1}, \quad (14)$$

$$R_2=\sqrt{R_{\mathrm{e}}^2+\left(R_{\mathrm{e}}+h_{\mathrm{t}}\right)^2-2R_{\mathrm{e}}\left(R_{\mathrm{e}}+h_{\mathrm{t}}\right)\cos\Phi_2}. \quad (15)$$

Similarly, the relationship between θ_1 and θ_2 can be calculated by $\triangle ABC$. We have

$$\theta_1+\left|\theta_2\right|=\arccos\frac{R_1^2+R_{\mathrm{d}}^2-R_2^2}{2R_1R_{\mathrm{d}}}. \quad (16)$$

From the above formula, ΔR and θ_2 can be easily obtained:

$$\Delta R=R_1+R_2-R_{\mathrm{d}}, \quad (17)$$

$$\theta_2=\theta_1-\arccos\frac{R_1^2+R_{\mathrm{d}}^2-R_2^2}{2R_1R_{\mathrm{d}}}. \quad (18)$$

2.2 Surface reflection coefficient analysis

According to the electromagnetic scattering theory, the surface reflection coefficient ρ depends on the working frequency, type of surface, polarization of the signal, surface roughness, etc. It can be expressed as (Lo and Litva, 1991)

$$\rho=\rho_{\mathrm{o}}\rho_{\mathrm{s}}D, \quad (19)$$

where ρ_{o}, ρ_{s}, and D are the smooth surface reflection coefficient, rough surface factor, and divergent factor, respectively. The smooth surface reflection coefficient ρ_{o} is generally divided into horizontal and vertical polarizations (Beckmann and Spizzichino, 1987; Mahafza, 2013), as

$$\rho_{\mathrm{o}}=\begin{cases}\dfrac{\sin\gamma-\sqrt{\varepsilon_{\mathrm{c}}-\cos^2\gamma}}{\sin\gamma+\sqrt{\varepsilon_{\mathrm{c}}-\cos^2\gamma}}, & \text{horizontal,}\\ \dfrac{\varepsilon_{\mathrm{c}}\sin\gamma-\sqrt{\varepsilon_{\mathrm{c}}-\cos^2\gamma}}{\varepsilon_{\mathrm{c}}\sin\gamma+\sqrt{\varepsilon_{\mathrm{c}}-\cos^2\gamma}}, & \text{vertical,}\end{cases} \quad (20)$$

where γ is the glancing angle, as

$$\gamma = \frac{1}{2}\left(\pi - \arccos\frac{R_1^2 + R_2^2 - R_d^2}{2R_1R_2}\right), \tag{21}$$

and ε_c is the complex dielectric constant related to the reflection surface. The rough surface factor ρ_s is given by (Lo and Litva, 1991)

$$\rho_s = e^{-z}, \tag{22}$$

where

$$z = \begin{cases} 2(2\pi\eta)^2, & \eta \le 0.1 \text{ rad}, \\ 0.16\eta^2 + 7.42\eta + 0.0468, & \text{otherwise}, \end{cases} \tag{23}$$

$$\eta = \frac{\sigma_h}{\lambda}\sin\psi_s, \tag{24}$$

and σ_h is the root-mean-squared value of the reflection surface. The divergent factor D is given by (Lo and Litva, 1991)

$$D \approx \frac{1}{\sqrt{1 + \dfrac{2G_1G_2}{R_eG\sin\psi_s}}}. \tag{25}$$

3 Target height and multipath attenuation joint estimation

For complex scenarios where the reflection condition is unknown, θ_2, ρ, and φ cannot be accurately calculated. This will result in performance degradation and even failure of conventional height estimation algorithms. Next, we analyze these three parameters in detail.

3.1 Incident angle of the reflected signal θ_2

For a far-field target, the direct wave ray is approximately parallel to the reflected ray in the case of low antenna height. The reflection area is very close to the radar. Thus, the reflection on the radar side can be approximated by plane reflection. Then, we obtain the approximation of

$$\theta_2 = -\theta_1. \tag{26}$$

Fig. 2 shows the difference between $|\theta_2|$ and θ_1 against the target elevation angle. Consider a digital array radar equipped with a uniform linear array. Set h_r=5 m and R_d=100 km. It can be seen that the difference between $|\theta_2|$ and θ_1 can be negligible. The above approximation is acceptable. Therefore, in the following discussion, we believe that Eq. (26) holds.

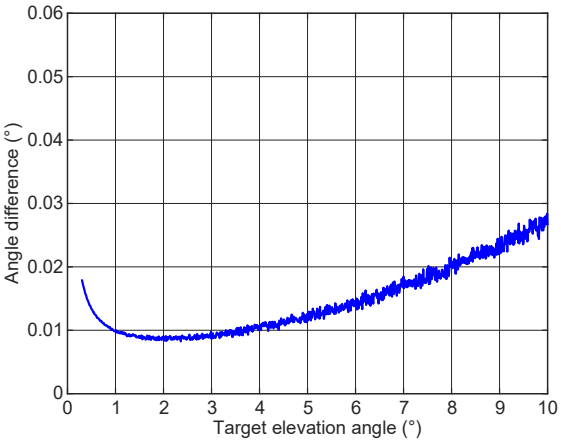

Fig. 2 The angle difference against the target elevation angle

3.2 Surface reflection coefficient ρ

The surface reflection coefficient ρ can be divided into amplitude and phase, as

$$\rho = \rho_A\rho_\psi = \rho_A e^{j\psi}, \tag{27}$$

where ρ_A denotes the amplitude of the surface reflection coefficient, and ψ denotes its phase. The precise ρ_A and ψ are difficult to obtain. For vertical polarization, ψ varies with the glancing angle, but for horizontal polarization, ψ is close to 180°. In complex scenarios, an error in ψ results in reduction of the target height estimation performance, but the approximate value of the phase for horizontal polarization can play a role in estimating ρ_A. Fortunately, horizontal polarization is often used for low-angle tracking. Thus, we discuss mainly the case of horizontal polarization.

Consider a digital array radar equipped with a uniform linear array with M elements where the distance between two adjacent array elements is d. Ignoring the effect of noise and assuming that there is no reflected signal, the signal received by array radar can be written as

$$\boldsymbol{x} = \alpha\boldsymbol{a}(\theta_1), \tag{28}$$

which shows that there is no relationship between the signal and the reflection coefficient. Next, ignoring

the effect of noise and assuming the existence of a reflected signal, the signal received by array radar can be written as

$$\boldsymbol{x} = \alpha\left[\boldsymbol{a}(\theta_1) + \rho \mathrm{e}^{-\mathrm{j}\varphi}\boldsymbol{a}(\theta_2)\right]. \tag{29}$$

Then, we obtain the amplitude of $\boldsymbol{x}$:

$$|\boldsymbol{x}| = |\alpha|\sqrt{\left(1+|\rho|^2\right)\boldsymbol{e}_M + 2|\rho|\boldsymbol{\beta}}, \tag{30}$$

where $\boldsymbol{e}_M = [1, 1, \cdots, 1]^{\mathrm{T}} \in \mathbb{C}^M$, and

$$\boldsymbol{\beta} = \cos\left\{\frac{2\pi d\left(\sin\theta_1 - \sin\theta_2\right)\boldsymbol{m}}{\lambda} + \left[\rho_\psi - \frac{4\pi h_{\mathrm{r}}\sin\theta_1}{\lambda}\right]\boldsymbol{e}_M\right\}, \tag{31}$$

$$\boldsymbol{m} = \left[-\frac{M-1}{2}, -\frac{M-3}{2}, \cdots, \frac{M-1}{2}\right]^{\mathrm{T}}. \tag{32}$$

Eq. (30) shows that $|\boldsymbol{x}|$ depends on the reflection coefficient, target elevation angle, and antenna height. To distinguish the spectrum of Eq. (30) from the case where there is no reflected signal, we normalize Eq. (30) and take the normalized result minus the mean of itself, as

$$\boldsymbol{X} = \frac{|\boldsymbol{x}|}{\max|\boldsymbol{x}|}, \tag{33}$$

$$\boldsymbol{y} = \boldsymbol{X} - \frac{1}{M}\sum_{i=1}^{M} X_i \boldsymbol{e}_M, \tag{34}$$

where $\boldsymbol{X} \in \mathbb{C}^M$, X_i denotes the i^{th} element of $\boldsymbol{X}$. Next, we take $\boldsymbol{y}$ as a time series and obtain the spectrum of $\boldsymbol{y}$ by the Fourier transform, as

$$F(k) = \sum_{i=0}^{N-1} y_i \mathrm{e}^{-\mathrm{j}\frac{2\pi ik}{M}}, k = 1, 2, \cdots, N, \tag{35}$$

where y_i denotes the i^{th} element of $\boldsymbol{y}$, y_i=0, i=M, M+1, ⋯, N, N is the number of samples of the Fourier transform, and $F(k)$ denotes the k^{th} element of $\boldsymbol{F}$. Then, we obtain the maximum element of $\boldsymbol{F}$ as

$$Q = \max|\boldsymbol{F}|. \tag{36}$$

We call Q the multipath characteristic value (MCV), which depends on the reflection coefficient, target elevation angle, and antenna height. Although the target elevation angle cannot accurately be known, the rough estimate of the elevation angle can be used as a priori knowledge. The details of rough estimation of the elevation angle will be discussed in Section 3.4. The error of ψ and the antenna height are generally acceptable for the estimation of ρ_{A}. In addition, a small error in ρ_{A} has little effect on the performance of height estimation (Wang et al., 2016). Then MCV depends only on ρ_{A}, so we can establish the relationship between MCV and ρ_{A} to estimate ρ_{A}. More concretely, the estimate of ρ_{A} can be written as

$$\hat{\rho}_{\mathrm{A}} = \begin{cases} 0, & \bar{\rho}_{\mathrm{A}} \le 0.2, \\ \bar{\rho}_{\mathrm{A}}, & \text{otherwise}, \end{cases} \tag{37}$$

where $\bar{\rho}_{\mathrm{A}}$ is the direct estimate of ρ_{A} by the relationship between MCV and ρ_{A}. We set $\hat{\rho}_{\mathrm{A}}$ to zero when $\bar{\rho}_{\mathrm{A}}$ is less than or equal to the empirical value of 0.2, because we believe that this is caused by the influence of noise. Note that the empirical value 0.2 is derived from data processing experience. Small adjustments to the empirical value generally do not affect the height estimation performance.

Consider a digital array radar equipped with a uniform linear array with 16 elements where the distance between two adjacent array elements is 0.5 m. Set h_{r}=5 m, R_{d}=100 km, h_{t}=3500 m, λ=1 m, and α=1. The amplitudes of the signals without noise against the number of array elements are shown in Fig. 3. From Fig. 3, it can be observed that the amplitude

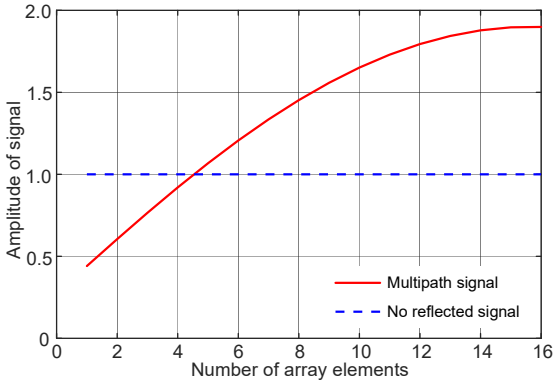

Fig. 3 The amplitude of signal against the number of array elements

of the multipath signal varies with the number of elements. Next, set N=128. The spectrum amplitude of $\boldsymbol{y}$ and the case where there is no reflected signal are shown in Fig. 4. There is a distinct difference in the maximum values of the spectrum amplitude between the two cases. The steps for estimation of ρ_{A} are summarized in Algorithm 1.

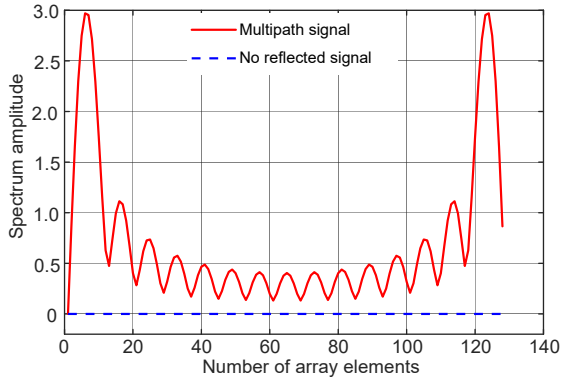

Fig. 4 The spectrum amplitude against the number of array elements

Algorithm 1 Estimation of ρ_{A}

Step 1: Set system parameters and obtain the rough estimate of the elevation angle.

Step 2: According to Eq. (29), establish the signal model.

Step 3: According to Eq. (36), calculate the MCV varying with ρ_{A}.

Step 4: According to Eq. (36), calculate the MCV of real data.

Step 5: Obtain $\bar{\rho}_{\mathrm{A}}$ by the results of steps 4 and 5, and obtain $\hat{\rho}_{\mathrm{A}}$ by Eq. (37).

3.3 Phase difference between direct and reflected signals

The phase difference between the direct and reflected signals φ is a very important parameter for height estimation. The antenna height can be searched as an unknown parameter to obtain the phase difference (Wang et al., 2016). However, there is also an error in the phase of the surface reflection coefficient ψ. From Eq. (5), it can be seen that the effects of φ and ψ on the signal are equivalent. Thus, we treat them as the same part, called multipath phase attenuation. Then, the composite array steering vector can be written as

$$\boldsymbol{w}(\theta_1,\phi)=\boldsymbol{a}(\theta_1)+\left|\rho\right|\mathrm{e}^{\mathrm{j}\phi}\boldsymbol{a}(-\theta_1), \tag{38}$$

where $\phi=\psi-\varphi$ is the multipath phase attenuation.

3.4 Target height and multipath attenuation joint estimation by alternating projection

Previously, we analyzed the key factors that affect the performance of height estimation under complex reflecting surface conditions. The main idea of the proposed algorithm is to estimate the amplitude of the surface reflection coefficient first, and then to conduct a joint search for target height and multipath phase attenuation by AP.

The log-likelihood function can be written as (Zhu et al., 2017)

$$\boldsymbol{f}(\theta_1,\phi)=\boldsymbol{x}^{\mathrm{H}}\boldsymbol{P}_{\boldsymbol{w}}(\theta_1,\phi)\boldsymbol{x}, \tag{39}$$

where $[\cdot]^{\mathrm{H}}$ denotes the conjugate transpose operation, and

$$\boldsymbol{P}_{\boldsymbol{w}}(\theta_1,\phi)=\frac{\boldsymbol{w}(\theta_1,\phi)\boldsymbol{w}^{\mathrm{H}}(\theta_1,\phi)}{\boldsymbol{w}^{\mathrm{H}}(\theta_1,\phi)\boldsymbol{w}(\theta_1,\phi)}. \tag{40}$$

The ML estimates of the target elevation angle and multipath phase attenuation are the values corresponding to the largest peak in the amplitude of the function:

$$\left(\hat{\theta}_1,\hat{\phi}\right)=\arg\max_{\theta_1,\phi}\boldsymbol{f}\left(\theta_1,\phi\right). \tag{41}$$

It requires a lot of computation to solve the above problem directly. The AP technique reduces computation by iterative processing. The technique solves the one-dimensional maximization problem by fixing all the other parameters at every iteration. By Ziskind and Wax (1988), the algorithm must converge to a local maximum. The initial estimation method in Ziskind and Wax (1988) has good performance, which ensures that the local maximum is the global maximum.

First, for the initial estimation of θ_1, which is the rough estimation mentioned earlier, we use the method in Ziskind and Wax (1988) and take Eq. (26) into account. Then, we obtain the initial estimate of θ_1 as

$$\hat{\theta}_1^{(0)}=\arg\max_{\theta_1}\left(\boldsymbol{x}^{\mathrm{H}}\boldsymbol{P}_{\boldsymbol{A}}(\theta_1)\boldsymbol{x}\right), \tag{42}$$

where

$$\boldsymbol{P}_{\boldsymbol{A}}(\theta_1)=\boldsymbol{A}(\theta_1)\left[\boldsymbol{A}^{\mathrm{H}}(\theta_1)\boldsymbol{A}(\theta_1)\right]^{-1}\boldsymbol{A}^{\mathrm{H}}(\theta_1), \quad (43)$$

$$\boldsymbol{A}(\theta_1)=\left[a(\theta_1),a(-\theta_1)\right]. \quad (44)$$

Second, we use the method in Algorithm 1 to estimate the amplitude of the reflection coefficient. Then, we start the iteration to estimate the elevation angle. The estimate of ϕ at the $(k+1)^{\text{th}}$ iteration is obtained by

$$\hat{\phi}^{(k+1)}=\arg\max_{\phi}\left(\boldsymbol{x}^{\mathrm{H}}\boldsymbol{P}_{\boldsymbol{w}}\left(\hat{\theta}_1^{(k)},\phi\right)\boldsymbol{x}\right). \quad (45)$$

The estimate of θ_1 at the $(k+1)^{\text{th}}$ iteration is obtained by

$$\hat{\theta}_1^{(k+1)}=\arg\max_{\theta_1}\left(\boldsymbol{x}^{\mathrm{H}}\boldsymbol{P}_{\boldsymbol{w}}\left(\theta_1,\hat{\phi}^{(k+1)}\right)\boldsymbol{x}\right). \quad (46)$$

Next, from the idea of AP, we repeat the above iteration process until the results of the two adjacent iterations are the same.

Note that when $\bar{\rho}_{\mathrm{A}}$ is less than 0.2, $\hat{\rho}_{\mathrm{A}}$ will be set to zero. That is, there is no reflected signal in the target echo. Thus, the estimate of θ_1 can be obtained directly by

$$\hat{\theta}_1=\arg\max_{\theta_1}\left\|\boldsymbol{a}(\theta_1)\boldsymbol{x}\right\|_2^2, \quad (47)$$

where $\|\cdot\|_2$ denotes the 2-norm. Finally, we calculate the target height $\hat{h}_{\mathrm{t}}$ by Eq. (6). The proposed algorithm is summarized in Algorithm 2.

Algorithm 2 The proposed algorithm

Step 1: Estimate the initial $\hat{\theta}_1^{(0)}$ by Eq. (42).

Step 2: Obtain $\bar{\rho}_{\mathrm{A}}$ by the method in Algorithm 1.

Step 3: If $\bar{\rho}_A \le 0.2$, set $\hat{\rho}_{\mathrm{A}}=0$ and go to step 4; otherwise, set $\hat{\rho}_{\mathrm{A}}=\bar{\rho}_{\mathrm{A}}$ and go to step 5.

Step 4: Estimate the target elevation angle $\hat{\theta}_1$ by Eq. (47), and go to step 8.

Step 5: Estimate the multipath phase attenuation $\hat{\phi}^{(k+1)}$ by Eq. (45).

Step 6: Estimate the target elevation angle $\hat{\theta}_1^{(k+1)}$ by Eq. (46).

Step 7: If the results of the two adjacent iterations are the same, stop the iteration; otherwise, set $k=k+1$ and go to step 5.

Step 8: Calculate the target height $\hat{h}_{\mathrm{t}}$ by Eq. (6).

4 Cramer-Rao bound

Assume that there are L discrete samples of the target echo. Based on the above analysis, the signal received by array radar can be written as

$$\boldsymbol{x}(l)=\alpha(l)\boldsymbol{w}(\theta_1,\phi)+\boldsymbol{n}(l), l=1,2,\cdots,L. \quad (48)$$

The log-likelihood function can be written as

$$\begin{aligned}T&=\ln\left\{P\left(\boldsymbol{x}(1),\cdots,\boldsymbol{x}(L);\left[\theta_1,\phi\right]\right)\right\}\\&=-\frac{L}{2}\ln(2\pi\sigma^2)-\frac{1}{2\sigma^2}\sum_{l=1}^{L}\Big[\left(\boldsymbol{x}(l)-\alpha(l)\boldsymbol{w}(\theta_1,\phi)\right)^{\mathrm{H}}\\&\quad\cdot\left(\boldsymbol{x}(l)-\alpha(l)\boldsymbol{w}(\theta_1,\phi)\right)\Big].\end{aligned} \quad (49)$$

The Fisher information matrix is given by

$$\boldsymbol{J}=\begin{bmatrix}J_{11}&J_{12}\\J_{21}&J_{22}\end{bmatrix}=\begin{bmatrix}-E\left\{\dfrac{\partial^2 T}{\partial\theta_1\partial\theta_1}\right\}&-E\left\{\dfrac{\partial^2 T}{\partial\theta_1\partial\phi}\right\}\\-E\left\{\dfrac{\partial^2 T}{\partial\phi\partial\theta_1}\right\}&-E\left\{\dfrac{\partial^2 T}{\partial\phi\partial\phi}\right\}\end{bmatrix}, \quad (50)$$

where

$$J_{11}=-\frac{L\alpha^2}{\sigma^2}\mathrm{real}\left(\frac{\partial\boldsymbol{w}^{\mathrm{H}}}{\partial\theta_1}\frac{\partial\boldsymbol{w}}{\partial\theta_1}\right), \quad (51)$$

$$J_{12}=J_{21}=-\frac{L\alpha^2}{\sigma^2}\mathrm{real}\left(\frac{\partial\boldsymbol{w}^{\mathrm{H}}}{\partial\phi}\frac{\partial\boldsymbol{w}}{\partial\theta_1}\right), \quad (52)$$

$$J_{22}=-\frac{L\alpha^2}{\sigma^2}\mathrm{real}\left(\frac{\partial\boldsymbol{w}^{\mathrm{H}}}{\partial\phi}\frac{\partial\boldsymbol{w}}{\partial\phi}\right), \quad (53)$$

$$\frac{\partial\boldsymbol{w}}{\partial\theta_1}=\boldsymbol{a}(\theta_1)*\boldsymbol{\eta}-\left|\rho\right|\mathrm{e}^{\mathrm{j}\phi}\boldsymbol{a}(-\theta_1)*\boldsymbol{\eta}, \quad (54)$$

$$\boldsymbol{\eta}=\left[\mathrm{j}\pi d\left[-(M-1),\cdots,(M-1)\right]\frac{\cos\theta_1}{\lambda}\right]^{\mathrm{T}}, \quad (55)$$

$$\frac{\partial\boldsymbol{w}^{\mathrm{H}}}{\partial\phi}=-\mathrm{j}\left|\rho\right|\mathrm{e}^{-\mathrm{j}\phi}\boldsymbol{a}(-\theta_1), \quad (56)$$

real$(\cdot)$ denotes the real part, and * denotes the Hadamard product. Define

$$\boldsymbol{H}=\boldsymbol{J}^{-1}=\begin{bmatrix}H_{11}&H_{12}\\H_{21}&H_{22}\end{bmatrix}. \quad (57)$$

We obtain the Cramer-Rao bound (CRB) of θ and ϕ as follows:

$$\begin{cases} \mathrm{CRB}_{\theta_1} = \sqrt{H_{11}}, \\ \mathrm{CRB}_{\phi} = \sqrt{H_{22}}. \end{cases} \tag{58}$$

In what follows, we show the estimated root-mean-squared error (RMSE) of the target elevation angle of the proposed algorithm and the CRB against the signal-to-noise ratio (SNR). We define SNR as

$$\mathrm{SNR} = \frac{LM|\alpha|^2}{\sigma^2}. \tag{59}$$

Set ρ to $0.9\mathrm{e}^{\mathrm{j}\pi}$. The other simulation conditions are the same as in Fig. 4. In the case of a single snapshot, the estimated RMSE of the target elevation angle of the proposed algorithm and the CRB against SNR are shown in Fig. 5. The estimated RMSE of the target elevation angle is smaller as SNR increases. The higher the SNR, the closer the estimated RMSE is to the CRB.

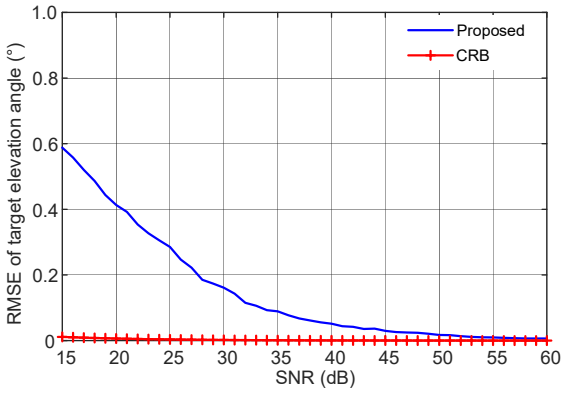

Fig. 5 RMSE of the target elevation angle against SNR

5 Simulation and real data processing results

5.1 Simulation results

In different scenarios, the proposed algorithm is compared with the RML algorithm (Lo and Litva, 1991), ML-AP algorithm (Ziskind and Wax, 1988), and height and reflection surface joint estimation (HRJE) algorithm (Wang et al., 2016). The processing methods of these four algorithms for key parameters are shown in Table 1.

Consider a digital array radar equipped with a uniform linear array with 16 elements where the distance between two adjacent array elements is d= 0.5 m. Set λ=1 m, h_r=5 m, and R_d=100 km. The number of Monte Carlo trials is set at 200 in all these simulations. All the following simulations follow the above conditions. These simulations are performed using MATLAB R2016b on a PC with Intel i7-7700, 3.60 GHz core frequency, and 8 GB RAM.

Table 1 The processing methods of four algorithms for key parameters

Parameter	RML	ML-AP	HRJE	Proposed
θ_1	Search	Search	Search	Search
h_r	Measurement	–	Search	–
θ_2	Calculation	Search	Calculation	$-\theta_1$
ρ_A	Calculation	–	Calculation	Estimation
ψ	Calculation	–	Calculation	Search $\phi=\psi-\varphi$
φ	Calculation	–	Calculation	

First, the ideal scenario with a smooth reflecting surface is considered. Set h_t=3500 m, $\rho=0.9\mathrm{e}^{\mathrm{j}\pi}$, and the target elevation angle is 1.67°. The RMSE of the target elevation angle and height against SNR of these algorithms mentioned earlier are shown in Figs. 6 and 7, for 64 snapshots and a single snapshot, respectively. For the case of 64 snapshots, the RML algorithm, ML-AP algorithm, and proposed algorithm perform Doppler filtering before height estimation. From Figs. 6 and 7, it can be seen that the RML algorithm is optimal and that the proposed algorithm performs better than the ML-AP algorithm and the HRJE algorithm in the ideal scenario. This is because the RML algorithm uses the most accurate information and the proposed algorithm tries its best to obtain the most accurate information. The running time of different methods for one Monte Carlo trial is shown in Table 2. The search region for the target elevation angle is [0.1°, 10°], and the search interval is 0.01°. The RML algorithm has the minimum running time because of the one-dimensional search of a single target. In the ML-AP algorithm, the direct and reflected signals are treated as two targets rather than two parts of the composite guide vector. The ML-AP algorithm has the maximum running time because of multiple one-dimensional searches of two targets. The HRJE algorithm and the proposed algorithm take less time than the ML-AP algorithm because of multiple one-dimensional searches of a single target. The proposed algorithm takes less time than the HRJE algorithm, because the proposed algorithm does not

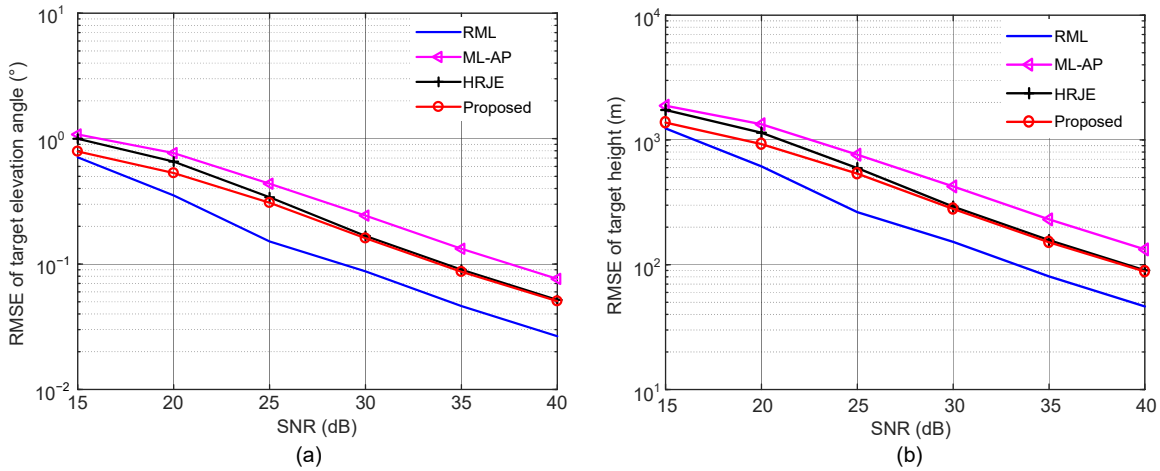

Fig. 6 RMSE of the target elevation angle (a) and target height (b) estimation against SNR with a smooth reflecting surface for 64 snapshots

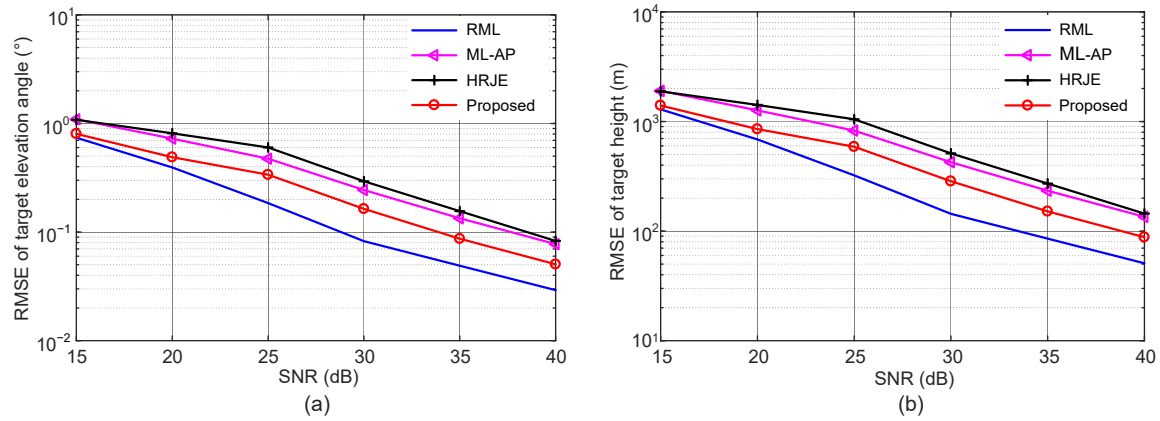

Fig. 7 RMSE of the target elevation angle (a) and target height (b) estimation against SNR with a smooth reflecting surface for a single snapshot

Table 2 Running time of different methods

Method	RML	ML-AP	HRJE	Proposed
Time (s)	0.005	1.162	0.157	0.039

need to calculate the phase difference between the direct and reflected signals φ.

Second, the complex scenario with an unknown reflecting surface is considered. Set $\rho=0.7e^{j\pi}$. Assume the error of h_r is 1 m, the error of ρ_A is 0.1, and the error of ρ_ψ is 10°. The radar receives only one snapshot. The RMSE of the target elevation angle and height against SNR of these algorithms mentioned earlier are shown in Figs. 8 and 9, for h_t=3500 m and h_t=7000 m, respectively. The target elevation angles for Figs. 8 and 9 are 1.67° and 3.10°, respectively. The performance of the RML algorithm is improved little with the increase of SNR because of the use of inaccurate information, and the three other algorithms are not so sensitive to the error. The proposed algorithm performs better than the other algorithms.

Then a more complex scenario with an unknown reflecting surface is considered. Set h_t=3500 m and $\rho=0.7e^{j\pi}$. Assume the error of h_r is 3 m, the error of ρ_A is 0.3, and the error of ρ_ψ is 30°. The radar receives only one snapshot. The RMSE of the target height against the SNR of these algorithms mentioned earlier is shown in Fig. 10. The performances of the RML algorithm and the HRJE algorithm are improved little with the increase of SNR. The performance of the HRJE algorithm is greatly reduced because of the large amplitude error of the reflection coefficient. Compared with other algorithms, the advantages of the

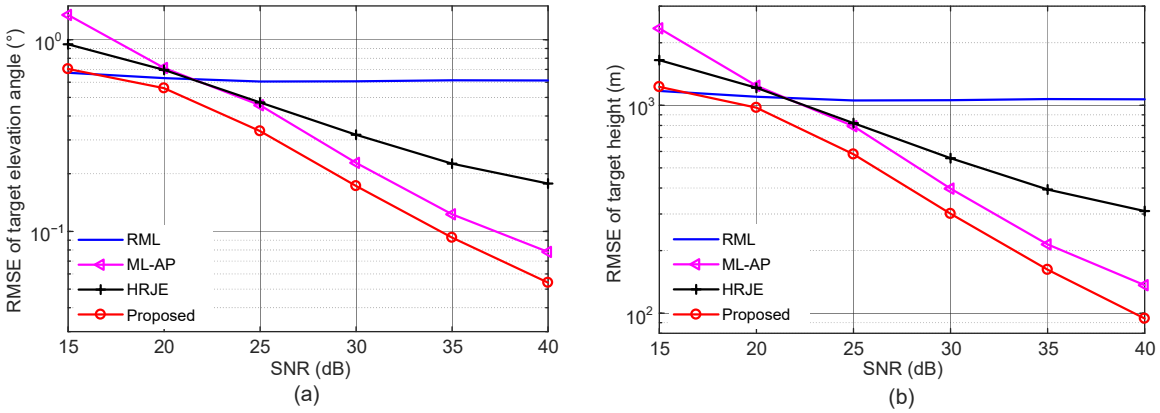

Fig. 8 RMSE of the target elevation angle (a) and target height (b) estimation against SNR with a complex reflecting surface for h_t=3500 m

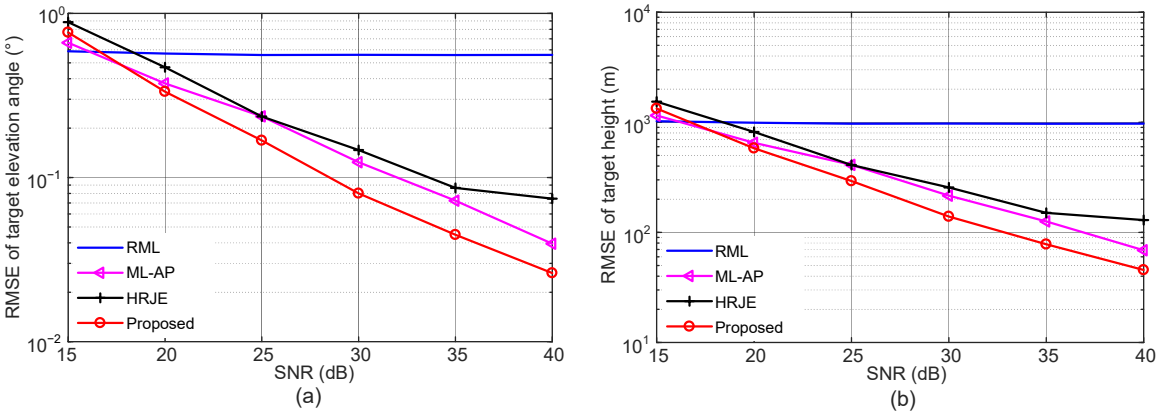

Fig. 9 RMSE of the target elevation angle (a) and target height (b) estimation against SNR with a complex reflecting surface for h_t=7000 m

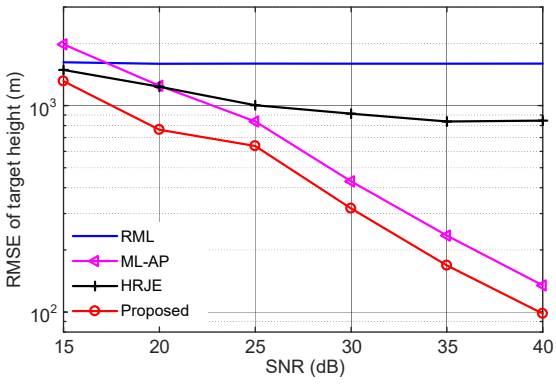

Fig. 10 RMSE of height estimation against SNR with a more complex reflecting surface for h_t=3500 m

proposed algorithm are more obvious in the more complex scenario.

Finally, a special scenario with an unknown reflecting surface is considered. Suppose that there is an obstacle blocking the reflected signal from entering the antenna at some time. That is to say, it is uncertain whether the reflected signal is included in a certain echo. Set h_t=3500 m and $\rho=0.9e^{j\pi}$. The radar receives only one snapshot. In the following simulation, whether the target signal contains the reflected signal is random in each Monte Carlo trial. The RMSE of the target height against the SNR of the algorithms is shown in Fig. 11. The conclusion is similar, and the performance of the proposed algorithm is also better than those of the others.

For the proposed algorithm, the number of iterations to convergence decreases with the increase of SNR. For example, it usually takes four iterations to obtain the result for 0 dB, three iterations for 20 dB, and only two iterations for higher SNR.

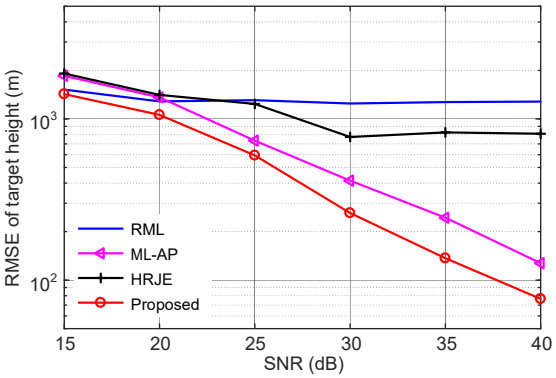

Fig. 11 RMSE of height estimation against SNR with an unknown multipath for h_t=3500 m

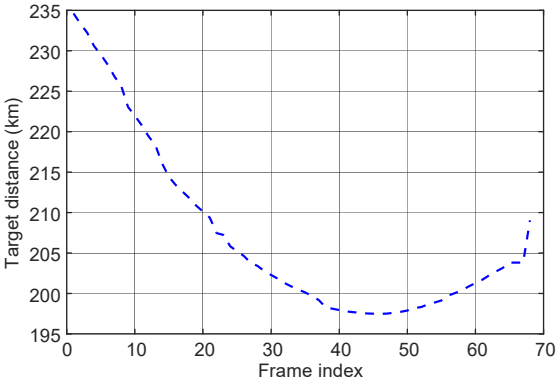

Fig. 12 Target distance against frames

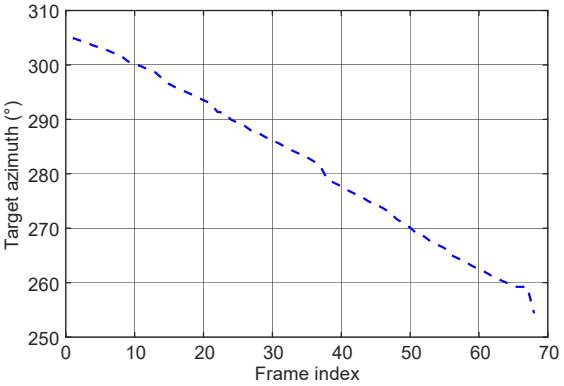

Fig. 13 Target azimuth against frames

5.2 Real data processing results

The real data under complex scenarios are applied to further verify the performance of the proposed algorithm. The array radar is equipped with a uniform linear array with 18 elements, where a distance between two adjacent array elements is d=0.55λ. The beam width is about 5.13°. The height of the reflecting surface and the surface reflection coefficient cannot be accurately obtained. The radar works in the meter wave band and receives only one snapshot. The real data are processed by pulse compression before height estimation.

The terrain scenario is a hilly area of great undulation. The target is an airplane that is first heading for the radar and then away from it. Figs. 12 and 13 show the target distance and azimuth change against frames, respectively. The distance between the airplane and radar first decreases from 235 km to 197 km and then increases to 210 km. Fig. 14 shows the processing results of the real data using RML, ML-AP, HRJE, and the proposed algorithm. The target elevation angle first increases from 1.3° to 2° and then decreases to 1.7°. The target height is about 9 km. It can be seen that the proposed algorithm has better performance in elevation angle and height estimations, and that the other algorithms have large estimation errors and less robustness. For the proposed algorithm, the number of iterations to convergence is two or three. In case of 2/3 of the frames, the elevation error of the proposed algorithm is less than 0.25°, that is, 1/20 of the beam width, and the height error is less than 1 km. In most frames, the elevation error of the proposed algorithm is less than 0.5°, that is, 1/10 of the beam width, and the height error is less than 2 km. Although the estimation error of the proposed algorithm is slightly larger at the 22nd and 61st frames, the overall advantage is still obvious.

6 Conclusions

In this paper, the problem of low-angle estimation for VHF radar with complex scenarios is discussed. The reflected signal is thought of as symmetric with respect to the horizontal plane of the direct signal. The amplitude of the surface reflection coefficient is estimated by the characteristic of the data itself, and it is considered that there is no reflected signal when the amplitude is very small. The phase of the surface reflection coefficient and the phase difference between the direct and reflected signals are searched as the same part, which is the multipath phase attenuation. Alternating projection is used to reduce computation.

The proposed algorithm fully exploits the characteristics of data in complex scenarios and improves

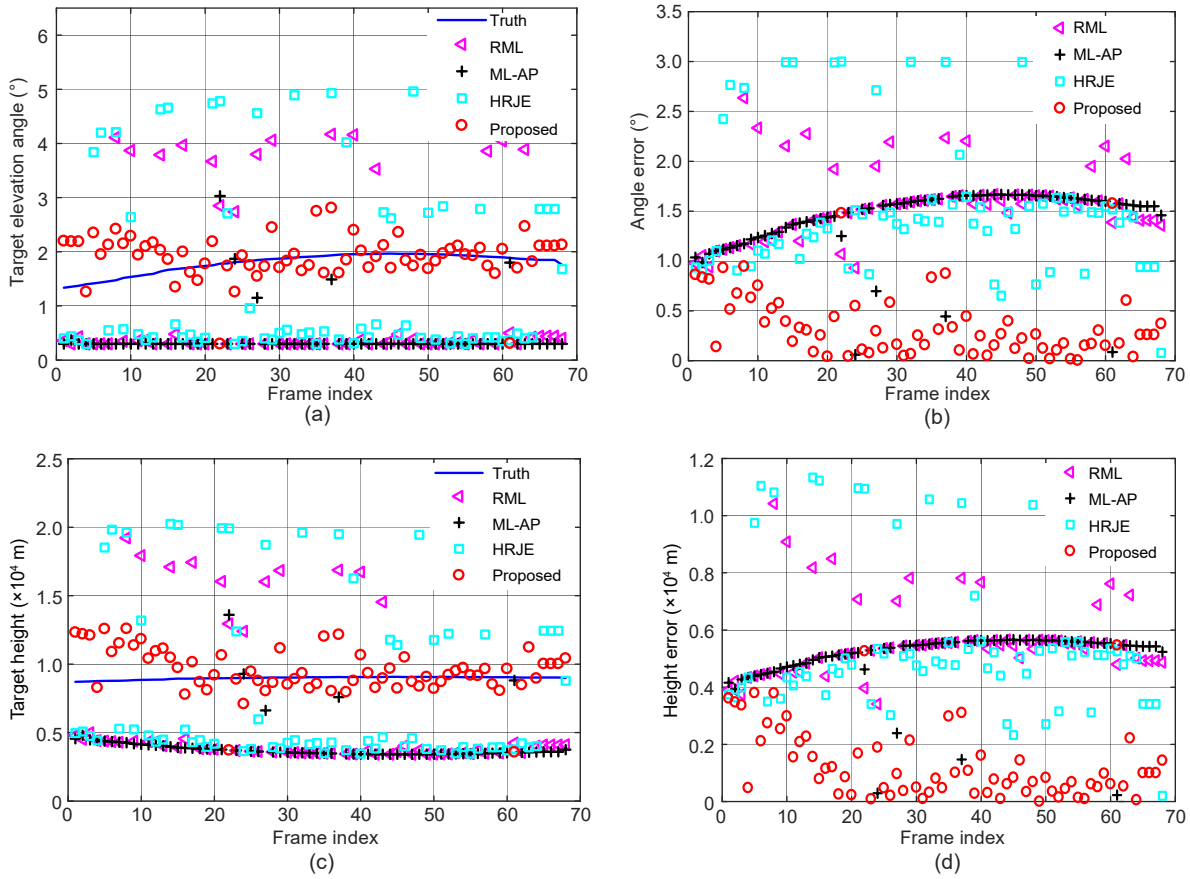

Fig. 14 Estimation of the target elevation angle (a), elevation angle error (b), target height (c), and height error (d) against frames

the performance of target height estimation. Computer simulations and real data processing results show the superiority of the proposed algorithm under complex scenarios, and the proposed algorithm works well with only one snapshot.

This paper discusses only the case of one target and one path reflection. In the case of multiple targets, the target echoes will affect each other. However, multiple targets can be separated in the range, Doppler, and angle dimensions by signal processing. If there are multiple targets in the same range unit, Doppler channel, and beam direction, the estimation performance will be degraded. In the case of multipaths, the signal model cannot match the actual data well. This will also lead to degradation of the estimation performance.

This paper discusses mainly the case of horizontal polarization. For vertical polarization, the amplitude of the surface reflection coefficient is still difficult to estimate.

This paper discusses the case where the absolute values of the incident angle and reflection angle are equal. In the case of high antenna height or a near field target, the absolute values of the incident angle and reflection angle are not equal. The reflection angle needs to be introduced as an unknown parameter, which greatly increases the complexity of the algorithm.

Contributors

Sheng CHEN designed the research. Sheng CHEN and Yongbo ZHAO processed the data. Sheng CHEN drafted the paper. Yili HU, Chenghu CAO, and Xiaojiao PANG helped organize the paper. Sheng CHEN and Yongbo ZHAO revised and finalized the paper.

Compliance with ethics guidelines

Sheng CHEN, Yongbo ZHAO, Yili HU, Chenghu CAO, and Xiaojiao PANG declare that they have no conflict of interest.

References

Ahn S, Yang E, Chun J, et al., 2010. Low angle tracking using iterative multipath cancellation in sea surface environment.

Proc IEEE Radar Conf, p.1156-1160. https://doi.org/10.1109/RADAR.2010.5494445

Ayasli S, 1986. SEKE: a computer model for low altitude radar propagation over irregular terrain. *IEEE Trans Antenn Propag*, 34(8):1013-1023. https://doi.org/10.1109/TAP.1986.1143933

Barton DK, 1974. Low-angle radar tracking. *Proc IEEE*, 62(6): 687-704. https://doi.org/10.1109/PROC.1974.9509

Beckmann P, Spizzichino A, 1987. The Scattering of Electromagnetic Waves from Rough Surfaces. Artech House, Norwood, USA.

Bosse E, Turner RM, Lecours M, 1991. Tracking Swerling fluctuating targets at low altitude over the sea. *IEEE Trans Aerosp Electron Syst*, 27(5):806-822. https://doi.org/10.1109/7.97326

Griesser T, Balanis C, 2003. Oceanic low-angle monopulse radar tracking errors. *IEEE J Ocean Eng*, 12(1):289-295. https://doi.org/10.1109/JOE.1987.1145238

Heylen R, Zare A, Gader P, et al., 2016. Hyperspectral unmixing with endmember variability via alternating angle minimization. *IEEE Trans Geosci Remote Sens*, 54(8):4983-4993. https://doi.org/10.1109/TGRS.2016.2554160

Lo T, Litva J, 1991. Use of a highly deterministic multipath signal model in low-angle tracking. *IEE Proc F (Radar Signal Process)*, 138(2):163-171. https://doi.org/10.1049/ip-f-2.1991.0022

Mahafza BR, 2013. Radar Systems Analysis and Design Using Matlab (3rd Ed.). CRC Press, Boca Raton, USA.

Park D, Yang E, Ahn S, et al., 2014. Adaptive beamforming for low-angle target tracking under multipath interference. *IEEE Trans Aerosp Electron Syst*, 50(4):2564-2577. https://doi.org/10.1109/TAES.2014.130185

Pillai SU, Kwon BH, 1989. Forward/backward spatial smoothing techniques for coherent signal identification. *IEEE Trans Acoust Speech Signal Process*, 37(1):8-15. https://doi.org/10.1109/29.17496

Roy R, Kailath T, 1989. ESPRIT-estimation of signal parameters via rotational invariance techniques. *IEEE Trans Acoust Speech Signal Process*, 37(7):984-995. https://doi.org/10.1109/29.32276

Schmidt RO, 1986. Multiple emitter location and signal parameter estimation. *IEEE Trans Antenn Propag*, 34(3): 276-280. https://doi.org/10.1109/TAP.1986.1143830

Shan TJ, Wax M, Kailath T, 1985. On spatial smoothing for direction-of-arrival estimation of coherent signals. *IEEE Trans Acoust Speech Signal Process*, 33(4):806-811. https://doi.org/10.1109/tassp.1985.1164649

Skolnik MI, 2008. Radar Handbook (3rd Ed.). McGraw-Hill, New York, USA.

Takahashi R, Hirata K, Maniwa H, 2010. Altitude estimation of low elevation target over the sea for surface based phased array radar. Proc IEEE Radar Conf, p.123-128. https://10.1109/RADAR.2010.5494639

Teti JG, 2000. Wide-band airborne radar operating considerations for low-altitude surveillance in the presence of specular multipath. *IEEE Trans Antenn Propag*, 48(2): 176-191. https://doi.org/10.1109/8.833067

Wang SH, Cao YH, Su HT, 2014. Joint estimation of the target height and the reflecting surface height in low angle radar. Proc 12th Int Conf on Signal Processing, p.1868-1871. https://doi.org/10.1109/ICOSP.2014.7015316

Wang SH, Cao YH, Su HT, et al., 2016. Target and reflecting surface height joint estimation in low-angle radar. *IET Radar Sonar Navig*, 10(3):617-623. https://doi.org/10.1049/iet-rsn.2015.0391

Xu ZH, Rao B, Xiong ZY, et al., 2013. Elevation finding algorithm in beam domain under multi-path environments for VHF radar. *IET Radar Sonar Navig*, 7(9):978-984. https://doi.org/10.1049/iet-rsn.2012.0221

Xu ZH, Huang T, Xiong ZY, et al., 2014. Low angle tracking algorithm using frequency diversity for array radar. *J Nat Univ Def Technol*, 36(2):93-98 (in Chinese). https://doi.org/10.11887/j.cn.201402016

Zhu YT, Zhao YB, Shui PL, 2017. Low-angle target tracking using frequency-agile refined maximum likelihood algorithm. *IET Radar Sonar Navig*, 11(3):491-497. https://doi.org/10.1049/iet-rsn.2016.0301

Ziskind I, Wax M, 1988. Maximum likelihood localization of multiple sources by alternating projection. *IEEE Trans Acoust Speech Signal Process*, 36(10):1553-1560. https://doi.org/10.1109/29.7543